Eur. Phys. J. D **24**, 283–286 (2003)
DOI: 10.1140/epjd/e2003-00160-3

THE EUROPEAN PHYSICAL JOURNAL D

Hyperthermal surface-collisions of water cluster cations

W. Christen[1,a] and U. Even[2]

[1] Humboldt-Universität zu Berlin, Institut für Chemie, Brook-Taylor-Str. 2, 12489 Berlin, Germany
[2] Tel Aviv University, Sackler Faculty of Exact Sciences, School of Chemistry, Ramat Aviv, Tel Aviv 69978, Israel

Received 10 September 2002
Published online 3 July 2003 –

Abstract. Size-selected, protonated water cluster cations $(H_2O)_nH^+$, $4 \leq n \leq 32$, are scattered at normal incidence from the surface of a diamond-coated silicon wafer at collision energies $0 \leq E_{\rm coll} \leq 500$ eV. The size distribution of collision-induced fragment-ions and the ion yield of scattered particles are analyzed, using a secondary time-of-flight mass spectrometer, as a function of the cluster size, n, and the collision energy, $E_{\rm coll}$. Even at low impact energies only very small fragment-ions can be detected, with a maximum fragment size of ∼35% of the colliding parent cluster ions. For clusters consisting of more than 10 molecules, the protonated water dimer $(H_2O)_2H^+$ becomes the predominant fragment-ion. The total charge survival yield obeys a nonlinear increase with cluster size; for the largest clusters investigated, more than 35% of the impacting ions survive the surface collision in the cationic charge state.

PACS. 34.30.+h Intramolecular energy transfer; intramolecular dynamics; dynamics of van der Waals molecules – 34.50.-s Scattering of atoms and molecules – 34.70.+e Charge transfer – 36.40.-c Atomic and molecular clusters – 61.46.+w Nanoscale materials: clusters, nanoparticles, nanotubes, and nanocrystals – 82.40.-g Chemical kinetics and reactions: special regimes and techniques

1 Introduction

In the area of particle-surface interactions, one of the most interesting topics is the impact of clusters on a solid target, due to a number of unique chemical and physical properties [1]. Cluster-surface impact processes can result in the deposition of significant amounts of energy in a small, localized region and may exhibit collective phenomena that are not seen for individual molecule-surface collisions.

In the present study we investigate the fragmentation and neutralization of size-selected, protonated water cluster cations $(H_2O)_nH^+$, colliding with a solid, nonreactive diamond surface at kinetic energies up to 30 eV per molecule. Time-of-flight mass spectrometry is used to obtain quantitative fragment-ion abundances as a function of the cluster size and the impact energy.

2 Experimental setup

The experimental configuration (Fig. 1) used for our measurements consists of a pulsed cluster-ion source, a primary time-of-flight mass spectrometer, two pulsed mass-gates, and an ultrahigh vacuum target collision chamber containing a secondary time-of-flight mass spectrometer for fragment-ion analysis [2].

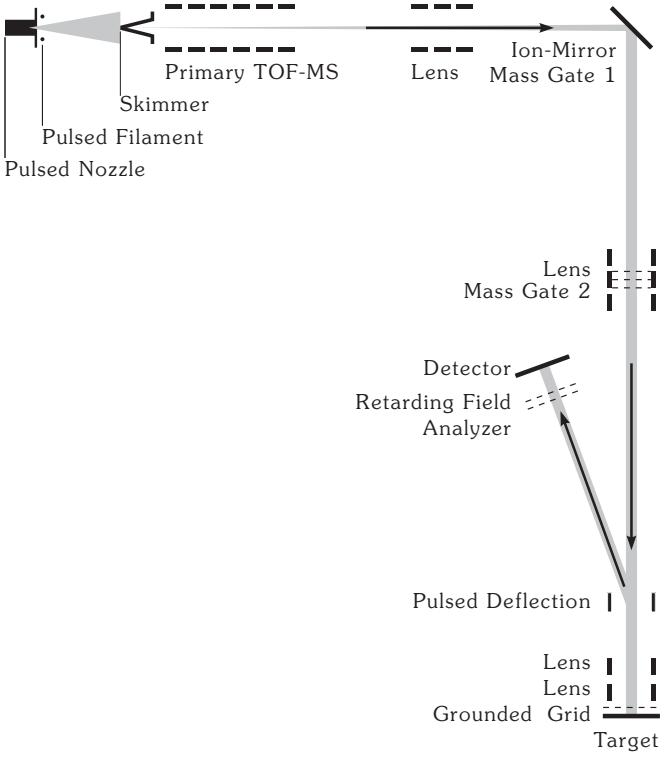

Fig. 1. Sketch of the experimental setup.

[a] e-mail: cluster@wolfgang-christen.net

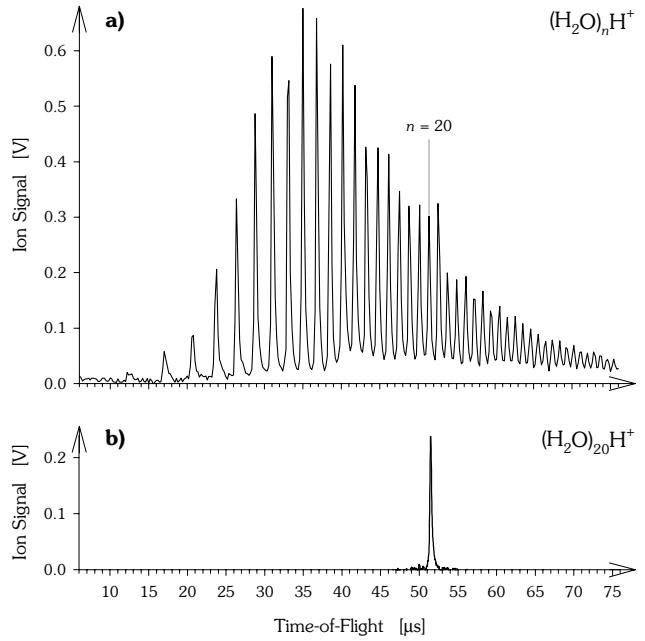

Fig. 2. (a) Primary time-of-flight mass spectrum of protonated water cluster ions, $(H_2O)_nH^+$, measured at the target surface with a home-built current amplifier. Ion optical parameters are optimized for the specific cluster size investigated, here $n = 20$. Note the pronounced change in cluster ion intensity from $(H_2O)_{21}H^+$ to $(H_2O)_{22}H^+$ due to the second solvation shell. (b) Mass selection of the cluster ion beam employing two sequential mass-gates.

Protonated water cluster ions, $(H_2O)_nH^+$ (Fig. 2a), are efficiently generated by pulsed, supersonic expansion of water vapor (vapor pressure at room temperature) diluted in a carrier gas (70% He, 30% Ne, 5 MPa stagnation pressure), and subsequent ionization by electrons emitted from a pulsed filament ($\simeq$ 90 eV, 10 μs voltage pulse). The jet source consists of a newly designed, home-built high pressure valve [3] that allows for an ultrashort pulse width (10−15 μs), together with a much improved pulse-to-pulse stability. The expanding jet is collimated by a skimmer (6 mm diameter), and arrives at the primary time-of-flight mass spectrometer, a modified Wiley-McLaren type. Here ions are accelerated to a translational energy of about 1.9 keV. A first mass selection of the cluster-ion beam is achieved by pulsing the high voltage applied at a planar ion mirror, deflecting cluster ions by 90° into the UHV scattering chamber. Mass selectivity is further improved by a second mass-gate, acting as a high-pass filter, while the ion mirror serves as a low-pass/band-pass filter. This sequential configuration avoids too short high voltage pulse durations and allows for an improved mass selection of cluster ions.

Mass selected water cluster ions (Fig. 2b) are guided at normal incidence towards the surface of a silicon target, which is coated with an electrically conductive ($\simeq$ 80 $\Omega\,\mathrm{cm}^{-1}$), $\simeq$ 10 μm thick p-type diamond film. Adsorption of water films on the target surface is minimized by constantly heating the sample to $\simeq$ 400 K from the rear side with a 50 W halogen lamp. Prior to impact, cluster ions are decelerated to the desired collision energy by the use of a retarding field between a grounded, laser-etched grid and the target surface, to which a high voltage is applied. The same high field ($\simeq 2 \times 10^6$ V m^{-1}) that decelerates incoming cluster ions also efficiently collects and reaccelerates scattered ions. Because impacting ions are temporally focussed onto the target surface (temporal half-width $\Delta t \simeq 100$ ns), the reacceleration allows a mass analysis of fragment-ions through their time-of-flight from the target to the detector. A main design element of the experimental configuration is the normal incidence of ions with an extraordinarily short distance used for de- and reacceleration. As has been verified by SIMION trajectory calculations, this distinct feature allows to collect virtually all ions leaving the target surface. Primary and secondary time-of-flight mass spectra are acquired using a digitizing storage oscilloscope, averaging 256 ion pulses for an improved signal-to-noise ratio.

3 Results and discussion

The collision energy of the parent cluster cations, E_{coll}, is given by the difference between the mean kinetic energy of the impinging ions E_{i} (with a typical kinetic energy spread $\Delta E_{\mathrm{i}} \simeq 10$ eV, and $\Delta E_{\mathrm{i}}/E_{\mathrm{i}} < 1\%$), and the voltage applied to the silicon target U_{target}, $E_{\mathrm{coll}} = E_{\mathrm{i}} - eU_{\mathrm{target}}$. If the target potential is higher than the kinetic energy of the incident ions, they will be reflected elastically without hitting the target surface. This feature allows the detection of the primary cluster-ion beam (Fig. 3a), and a direct, quantitative measurement of the charge survival yield. For lower target potentials, $eU_{\mathrm{target}} < E_{\mathrm{i}}$, cluster ions will impact on the target surface, leading — *inter alia* — to charge transfer processes and collision-induced fragmentation.

Two examples of secondary time-of-flight mass spectra, resulting from the impact of $(H_2O)_{20}H^+$ cluster ions at different collision energies, are depicted in Figures 3b and 3c: parent cluster ions, and small fragment-ions such as the protonated water monomer, dimer, trimer, and tetramer can be detected. Their abundance strongly depends on the collision energy. In general, the size of the fragment-ions decreases for higher collision energies. In order to obtain the complete fragmentation pattern of impacting cluster ions, the collision energy is increased systematically by lowering the target voltage in small increments (voltage resolution $\Delta U_{\mathrm{target}} \simeq 1$ V). At very low impact energies the time-of-flight mass spectra are dominated by parent cluster ions (Fig. 3b). At higher impact energies the parent cluster-ion signal disappears, while small fragment-ions containing up to six water molecules can be observed (Fig. 3c). However, no large cluster fragment-ions, resulting from the loss of one (or few) neutral water monomers from the parent cluster, such as $(H_2O)_{18}H^+$, can be detected. At even higher collision energies ($E_{\mathrm{coll}} \geq 150$ eV) some sputtered hydrocarbon ions ($C_2H_2^+$, $C_3H_3^+$) can be observed. Visualizing the ion intensities as a two-dimensional contour plot (Fig. 4) reveals the

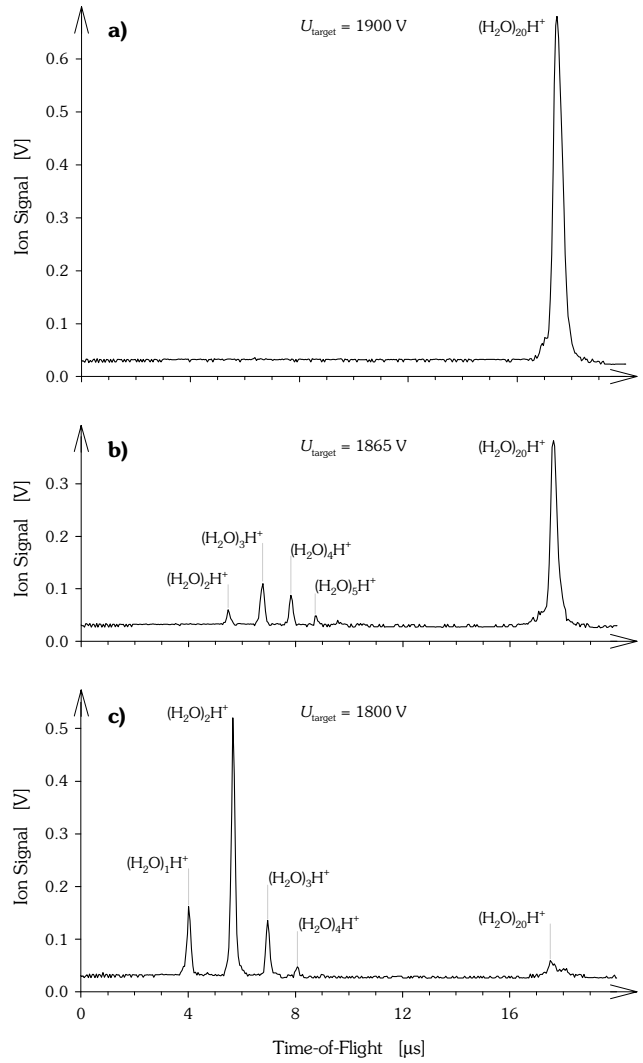

Fig. 3. Secondary time-of-flight mass spectra of $(H_2O)_{20}H^+$ clusters colliding with the diamond-coated silicon target, kept at different target potentials U_{target}. The temporal zero of the secondary time-of-flight spectra is given by the impact of the parent cluster ions on the target surface, as measured with a home-built current amplifier on the target (without any bias voltage applied), *cf.* Figure 2b. (a) Elastic reflection of incoming cluster ions. (b) "Soft" cluster impact, $E_{\mathrm{coll}} \simeq 0$ eV. (c) Energetic cluster impact, $E_{\mathrm{coll}} = 65$ eV.

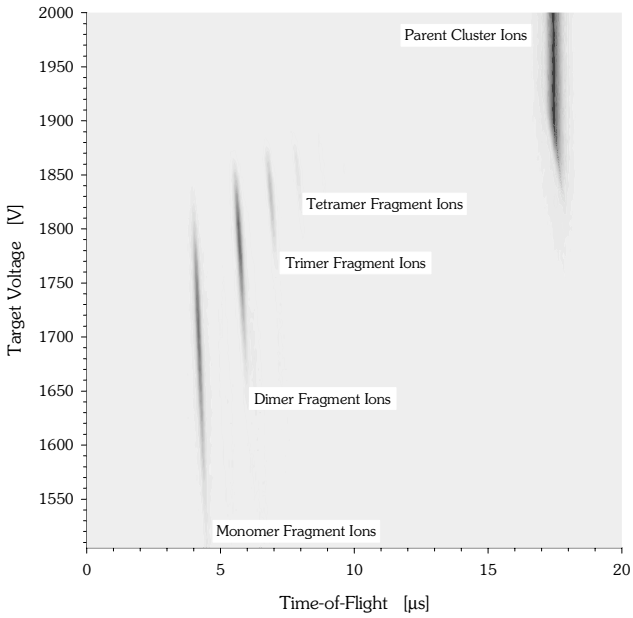

Fig. 4. Contour plot of the ion signal as a function of time-of-flight and target voltage, showing the transition from intact parent cluster ions to small molecular fragment-ions.

transition from intact parent cluster ions to small molecular fragment-ions (termed *shattering* [4–6]). Cluster-size specific fragmentation pattern, allowing a quantitative evaluation and the comparison of ion yields, are derived from these data sets by the following procedure: first, the collision-energy dependent time-of-flight mass spectra of a specific parent cluster size are integrated within a given time frame of a few hundred nanoseconds, corresponding to one specific particle size, as a function of the target voltage. After subtraction of offset voltages the resulting spectrum is normalized to the intensity of the incoming parent cluster ions (100%), and scaled to account for the velocity-dependent ion detection efficiency [7]. Finally the target voltage is converted to the collision energy using the mean kinetic energy of the primary cluster-ion beam (with a nearly Gaussian kinetic energy distribution [8]). Several individual data sets are averaged, and the energy dependence of the resulting fragmentation pattern is modelled using an asymmetrical Weibull distribution function. The outcome of this procedure is depicted in Figure 5, showing the fragmentation pattern of protonated clusters of 8 and 32 water molecules, respectively. Note that fragment-ions can be detected even at impact energies above 100 eV. While these ions will probably be very hot, they are stable at least on the time scale of reacceleration: the time t an ion leaving the target after impact spends between the target surface and the grounded grid, is given by

$$t = d\sqrt{\frac{m_{\mathrm{fragment}}}{2eU_{\mathrm{target}}}}$$

assuming a zero recoil velocity of the fragment-ion. d is the distance between the target surface and the grounded grid, with $d = 2$ mm. Thus, tetramers are stable at least for 27.5−31.8 μs, trimers for 23.9−27.6 μs, dimers for 19.6−22.6 μs, and monomers for 14.0−16.2 μs, depending on the collision energy.

Comparing the fragmentation pattern of different sizes of the parent cluster ion (Fig. 5a *vs.* Fig. 5b) it turns out that for larger parent cluster ions significantly more charged fragments can be detected. From these data the total fragment-ion yield can be derived by adding the individual fragment-ion intensities of Figure 5 as a function of the collision energy. The result is plotted in Figure 6: basically, for most collision energies, most ions are neutralized on surface impact. Only for the largest clusters investigated, slightly more than 35% of the impacting ions can

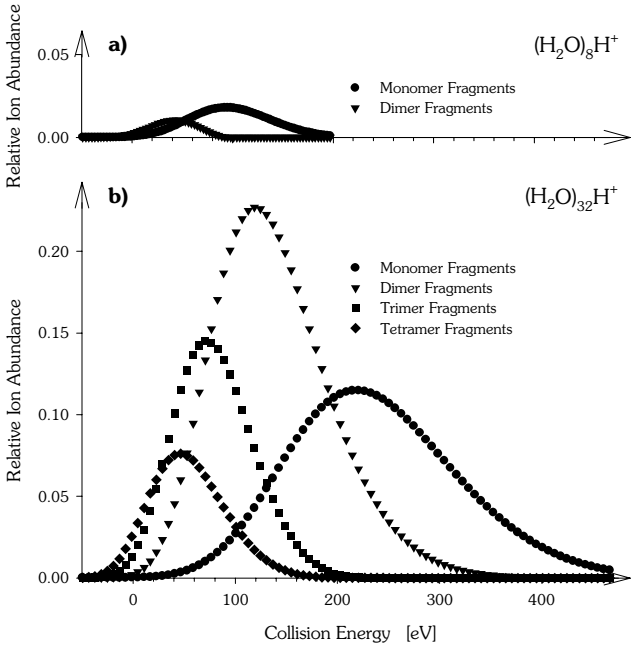

Fig. 5. Dependence of the fragment-ion abundance on parent cluster size and kinetic energy. (a) Impact of $(H_2O)_8H^+$. (b) Impact of $(H_2O)_{32}H^+$.

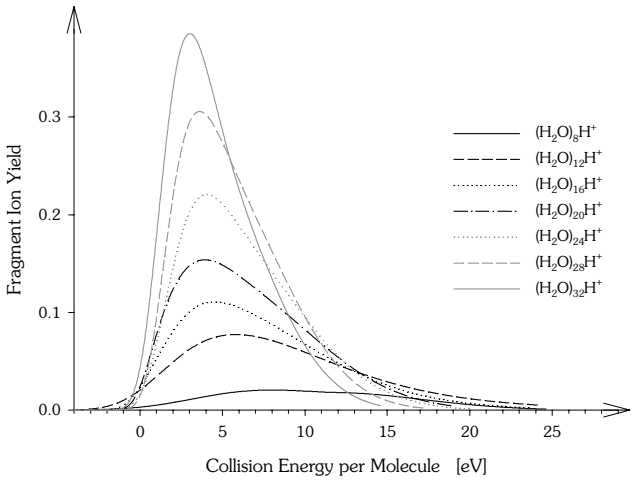

Fig. 6. Total fragment-ion yield as a function of the collision energy of the parent cluster ions, $(H_2O)_nH^+$, obtained by summation of the relative yields of the four dominant fragment-ions (monomer, dimer, trimer, tetramer). For larger clusters the highest fragment-ion yield is detected at collision energies of 3−4 eV/molecule.

survive the collision in the cationic charge state. The cluster size dependence of the maximum fragment-ion yield is shown in Figure 7 and can be best described by a fit of the functional form $Y \propto n^2$.

4 Summary

The surface-induced fragmentation of protonated water cluster cations is characterized by the *shattering* of the impacting parent cluster ions to small molecular fragment-ions. We especially note the absence of any fragment-ions of intermediate sizes or sizes close to the original parent cluster ions. The experimental setup with its highly efficient ion collection and detection scheme allows to determine the charge survival yield. It turns out that most parent cluster ions are neutralized on surface impact. For larger parent cluster ions, much more charged fragments can be observed than for smaller cluster ions. The total fragment-ion yield increases nonlinearly with cluster size, suggesting that the proton is solvated *within* the cluster, in analogy to [9]; for larger clusters its mean distance to the conductive target will increase, reducing the probability for electron transfer processes. The total fragment-ion yield exhibits its maximum at collision energies $E_{\rm coll} \simeq 100$ eV.

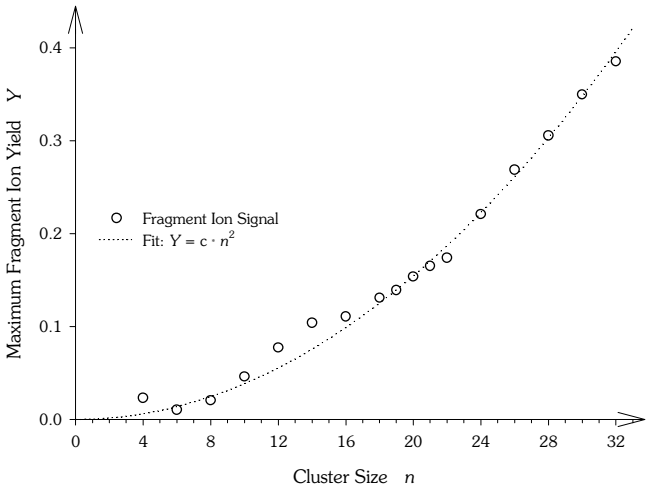

Fig. 7. The maximum of the (energy-dependent) total fragment-ion yield as a function of the size n of the impacting water cluster ions, $(H_2O)_nH^+$. The dotted line is a fit to the data points, see text.

We gratefully acknowledge financial support by a grant from GIF.

References

1. C.L. Cleveland, U. Landman, Science **257**, 355 (1992)
2. W. Christen, U. Even, Eur. Phys. J. D **16**, 87 (2001)
3. U. Even, J. Jortner, D. Noy, N. Lavie, C. Cossart-Magos, J. Chem. Phys. **112**, 8068 (2000)
4. T. Raz, U. Even, R.D. Levine, J. Chem. Phys. **103**, 5394 (1995)
5. E. Hendell, U. Even, T. Raz, R.D. Levine, Phys. Rev. Lett. **75**, 2670 (1995)
6. T. Raz, R.D. Levine, J. Chem. Phys. **105**, 8097 (1996)
7. H. Yasumatsu, S. Koizumi, A. Terasaki, T. Kondow, J. Chem. Phys. **105**, 9509 (1996)
8. W. Christen, U. Even, T. Raz, R.D. Levine, Int. J. Mass Spectrom. Ion Proc. **174**, 35 (1998)
9. H. Yasumatsu, A. Terasaki, T. Kondow, Int. J. Mass Spectrom. Ion Proc. **174**, 297 (1998)